Dalton Transactions

PAPER

View Article Online
View Journal | View Issue

Cite this: *Dalton Trans.*, 2015, **44**, 18065

Iron(II) spin crossover complexes with diaminonaphthalene-based Schiff base-like ligands: mononuclear complexes†

Charles Lochenie,[a] Julia Heinz,[a] Wolfgang Milius[b] and Birgit Weber*[a]

Received 7th August 2015,
Accepted 22nd September 2015

DOI: 10.1039/c5dt03048j

www.rsc.org/dalton

The synthesis of new Schiff base-like ligands with extended π-system and their iron complexes is described. Some of the iron(II) complexes with N-heterocycles as axial ligands show spin crossover behaviour. The influence of the extended aromatic system on cooperative interactions is investigated by single crystal X-ray structure analysis, X-ray powder diffraction, and magnetic measurements. A combination of C–H···π and C–H···O interactions is made responsible for up to 10 K wide thermal hysteresis loops.

Introduction

Molecular switches continue to attract the interest of synthetic chemists due to potential applications in the field of sensing or memory devices.[1] Iron(II) spin crossover (SCO) complexes belong to this class of molecular switches as they can be switched between the diamagnetic low-spin (LS) and the paramagnetic high-spin (HS) state.[2] This switching process can be triggered by many different means. Next to physical stimuli like temperature, pressure, or light irradiation, the interaction with guest molecules[3] (especially for porous materials) or phase transitions[4] (*e.g.* for SCO materials with liquid crystalline properties) can initiate the spin transition. Of the different types of spin transition (gradual, abrupt, step-wise, with hysteresis) a special focus is set on spin transition with hysteresis, as this gives rise to bistability (memory effect) over a certain temperature region. Cooperative spin transitions with hysteresis are usually only observed in the solid state (bulk material or nanostructured materials), however it was recently shown that such phenomenon is also observable in solution.[5] For the display of hysteretic behaviour, intermolecular interactions are needed in order to transfer the structural changes associated with the spin transition from one molecule to another. Different strategies can be used to realise those intermolecular interactions that were also applied to the Schiff base-like ligands used in our group. Building short contacts between the complex molecules is one strategy to design SCO complexes with hysteresis.[6] If wider hysteresis loops are desired, a combination of short range and long range interactions as it is often obtained for 1D coordination polymers or ladder-like compounds is promising.[7] In the last years we investigated in detail the impact of hydrogen bonds on the hysteresis width of SCO complexes.[8,9] One interaction we have not used in our iron(II) complexes so far is the π–π-interaction. However, there are examples in literature, where π-interactions between extended aromatic systems increase the width of the hysteresis loop. One series with the general composition $[Fe(L)_2NCS_2]$ (with L being a bidentate ligand 2,2′-bipyridine (bipy), phenantroline (phen), or dipyrido[3,2-*a*:2′3′-*c*]phenazine (dpp)) is discussed by Real and co-workers.[10] The systematic increase of the aromatic part of the ligand leads to improved π-stacking and by this to wider hysteresis loops. Indeed, for the dpp ligand a 40 K wide thermal hysteresis loop is observed.[11] Another example of a mononuclear complex with a 37 K wide hysteresis loop due to π-stacking was reported by Létard and co-workers.[12] Consequently we decided to modify our Schiff base-like ligands through the introduction of a naphthalene based ligand backbone. In Scheme 1, the general structure of the new ligands, their iron complexes, and the used abbreviations are given.

Results

Syntheses

The spin crossover (SCO) complexes were produced in a three-step synthesis, whose synthetic pathway is given in Scheme 1. Firstly the new naphthalene-based Schiff base-like ligands **H_2Lx** (**1–4**) were synthesised, then the precursor methanol complexes **$[FeLx(MeOH)_n]$** (**5–8**) were formed by reaction with iron(II) acetate, which were finally converted to the target SCO

[a]*Inorganic Chemistry II, Universität Bayreuth, Universitätsstraße 30, NW I, 95440 Bayreuth, Germany. E-mail: weber@uni-bayreuth.de*
[b]*Inorganic Chemistry I, Universität Bayreuth, Universitätsstraße 30, NW I, 95440 Bayreuth, Germany*

†Electronic supplementary information (ESI) available: Magnetic susceptibility measurements of compounds **9**, **13**, **16**, **17** and **18**; powder diffraction patterns of samples **6**, **12** and **14**, TGA measurement of **11** and ORTEP drawings of **19** and **20**. CCDC 1040373–1040380. For ESI and crystallographic data in CIF or other electronic format see DOI: 10.1039/c5dt03048j

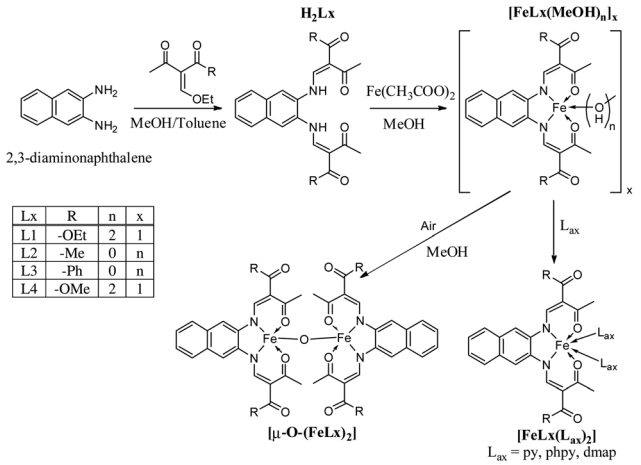

Lx	R	n	x
L1	-OEt	2	1
L2	-Me	0	n
L3	-Ph	0	n
L4	-OMe	2	1

Scheme 1 Pathway of synthesis of the SCO complexes described in this work and used abbreviations.

complexes **[FeL*x*(L$_{ax}$)$_2$]** (**9–18**). Oxidation of the intermediate complexes **[FeL*x*(MeOH)$_n$]** (**5–8**) in the air led to μ-oxido-bridged binuclear iron(III) complexes **[μ-*O*-(FeL*x*)$_2$]** (**19–20**).

Ligands. The synthesis of the ligands **H$_2$L*x*** (**1–4**) was achieved by condensing 2,3-diaminonaphthalene and the corresponding keto–enol ether following a modified method described by Wolf and Jäger.[13] The four new ligands were obtained in good yield as yellowish powder and their purity was checked with ^{1}H-NMR and elemental analysis. All ligands present characteristic ^{1}H-NMR doublet signals around 13 and 8.2–8.5 ppm, accounting for the protons of the –NH enamine and =C–H of the chelate cycles. The rest of the proton signals can be found in their respective expected region. IR spectra show two strong characteristic signals for the C=O vibrations, as well as a characteristic N–H band.

Methanol complexes [FeL*x*(MeOH)$_n$]. The precursor complexes **[FeL*x*(MeOH)$_n$]** (**5–8**) were synthesised by converting the equatorial Schiff base-like ligands **H$_2$L*x*** (**1–4**) with iron(II) acetate, with the acetate acting as a base for deprotonation of the equatorial ligand. IR spectra show that the C=O bands shift compared to the free ligand, in agreement with the coordination of an iron metal centre. Also the colour of the compounds drastically changes towards dark brown/black in the solid state. This is due to strong charge transfer between the iron centre and the ligand, as observed for similar compounds in literature.[14–16] It is usual for this type of complexes that two methanol molecules coordinate the iron(II) centre on axial positions, as shown for the phenyl-,[17,18] dialkoxyphenyl-[19,20] and dihydroxyphenyl-[21] derivatives of the same compound class. However, it was found by elemental analysis that for the naphthalene derivatives discussed in this manuscript the amount of coordinated methanol is depending on the substituents of the equatorial ligand. When the substituents are ester functions, like with L1 (R = –OEt) and L4 (R = –OMe), the complex will have two methanol coordinated to the iron centre. When the substituents are ketone functions, like L2 (R = –Me) and L3 (R = –Ph), no coordinating methanol was found. Those results were confirmed by the determination of the crystal structure of **[FeL2]**.

SCO complexes [FeL*x*(L$_{ax}$)$_2$]. For the observation of SCO, the crystal field strength needs to be shifted into the right region. Thus the coordination sphere of the Fe(II) centre was changed from FeN_2O_4 to FeN_4O_2 by placing strong *N*-coordinating ligands such as pyridine (py), 4-(dimethylamino)pyridine (dmap), or 4-phenylpyridine (phpy) on the axial positions. By combining the different equatorial ligands, whose substituents allow a fine tuning of the crystal field strength, and the three different axial ligands, ten new potential iron(II) SCO complexes could be synthesised. The synthesis of complexes [FeL1(py)$_2$] and [FeL3(phpy)$_2$] was not possible so far. The first complex precipitates as the pentacoordinated specie [FeL1(py)], while the later would not precipitate from the solution. The exact formula of the complexes was determined with elemental analysis and mass spectrometry. A list of the different complexes, along with their solvent content, is shown in Table 1.

Oxidation products. A crucial point during the synthesis is the identification of possible Fe(III) species produced during the synthesis of the SCO complexes. Therefore, mother liquors of the starting methanol complexes were left to slowly evaporate in the air. In the cases of compounds **5** and **8**, a few monocrystals of the corresponding μ-oxido-bridged binuclear iron(III) complexes **19** and **20** could be obtained. Those were sufficient for the analysis of the X-ray structures, however, the amount was too small for a further characterisation of the complexes.

Table 1 Overview of the SCO behaviour, characteristic $\chi_M T$ values [cm^3 K mol^{-1}], HS residue (γ_{HS}) at 50 K and the $T_{1/2}$ values [K]

	Compound	SCO behaviour	$\chi_M T$ (300 K)	$\chi_M T$ (50 K)	γ_{HS} (50 K)	$T_{1/2}$
9	[FeL2(py)$_2$]·2.5H$_2$O	HS	3.87	—	—	—
10	[FeL3(py)$_2$]·py	Abrupt	3.19	0.01	0	175
11	[FeL4(py)$_2$]·py	Two-step, gradual	2.90	0.84	0.29	150, 80
12	[FeL1(phpy)$_2$]	Hysteresis, 10 K	3.65	0.08	0	↓238, ↑248
13	[FeL2(phpy)$_2$]·2MeOH	HS	3.66	—	—	—
14	[FeL4(phpy)$_2$]	Hysteresis, 10 K	3.21	0.03	0	↓250, ↑260
15	[FeL1(dmap)$_2$]	Two-step, gradual, abrupt	3.12	0.10	0.03	224, 149
16	[FeL2(dmap)$_2$]	HS	3.39	—	—	—
17	[FeL3(dmap)$_2$]	HS	3.32	—	—	—
18	[FeL4(dmap)$_2$]	HS	3.31	—	—	—

Magnetism

The magnetic properties of the ten synthesised potential SCO complexes were investigated with a SQUID magnetometer, and are summarised in Table 1. Out of those complexes, five (samples **9**, **13**, **16**, **17**, **18**) are HS compounds with a $\chi_M T$ value around 3.3 cm^3 mol K^{-1} in the whole temperature range and no indication for SCO. The different values can be attributed to differences in the spin–orbit coupling. However, especially for the samples containing non-coordinating solvent molecules, small errors in the sample weight due to a solvent loss during the sample preparation are also possible. In the ESI, Fig. S1† the plot of $\chi_M T$ *vs.* T for those complexes is given. Compound **10** presents at 300 K a $\chi_M T$ value of 3.19 cm^3 K mol^{-1}, typical for iron(II) complexes in the HS state.[14–21,41] Upon cooling, this value remains constant down to 175 K where compound **10** undergoes a complete abrupt spin transition (ST) towards the LS state (top of Fig. 1). Below 160 K the $\chi_M T$ value stays constant with a value of 0.01 cm^3 K mol^{-1} until 10 K. Upon warming, the compound goes back to the HS state with the same $T_{1/2}$ of 175 K. The ST properties of **10** are stable upon several measurement cycles.

Compound **11** exhibits at 300 K a $\chi_M T$ value of 2.90 cm^3 K mol^{-1} which is in agreement with an iron(II) complex almost in the HS state (top of Fig. 1). Upon cooling, the $\chi_M T$ product stays constant until 170 K where compound **11** starts a gradual two-step SCO until 60 K, with T_1 and T_2, respectively, equal to 150 and 80 K. The SCO is incomplete with a residual HS fraction at 60 K of 0.29 ($\chi_M T$ = 0.84 cm^3 K mol^{-1}) which does not change down to 10 K. Upon warming, the compound **11** presents the same two-step transition towards the HS state at the same temperatures as upon cooling. When the compound is warmed above 380 K, the compound no longer exhibits SCO. Due to the conditions in the SQUID magnetometer (vacuum), uncoordinated as well as coordinated pyridine molecules could leave the sample, as already observed for other phenylene-based Fe(II) pyridine complexes.[19,22] The loss of pyridine was confirmed with a TGA measurement, which is shown in the ESI: Fig. S2.† As a result, the compound does not undergo SCO anymore upon cooling. This phenomenon could explain why a rather high HS fraction was observed for the original sample: a deficiency in pyridine in the powder, resulting from drying the compound under vacuum after the synthesis, could be responsible for the HS fraction at low temperature.

Compounds **12** and **14** show very similar SCO properties: at 300 K both present, with 3.65 and 3.21 cm^3 K mol^{-1}, typical magnetic susceptibility with temperature product values for iron(II) HS complexes (middle of Fig. 1). Upon cooling, both show a rather abrupt ST with $T_{1/2}\downarrow$ = 238 K and $T_{1/2}\downarrow$ = 250 K, respectively, for compound **12** and **14**.

Their $\chi_M T$ values at 50 K are with 0.08 and 0.03 cm^3 K mol^{-1} in agreement with an iron(II) LS centre, and stay constant until 10 K. Upon heating, both samples show an abrupt ST back to the HS state at, respectively, $T_{1/2}\uparrow$ = 248 K and $T_{1/2}\uparrow$ = 260 K, revealing for both samples a 10 K hysteresis. As compounds **12** and **14** only differ by one substituent on the equatorial ligand (–OEt for **12** and –OMe for **14**), and show the same SCO behaviour displaced by 12 K, one could see the direct influence of the substituents of the equatorial ligand on the crystal field strength of the complexes, but only if **12** and **14** are isostructural. The magnetic properties of **12** and **14** are stable upon heating until 400 K and can be cycled several times. This is a surprisingly high thermal stability for mono-

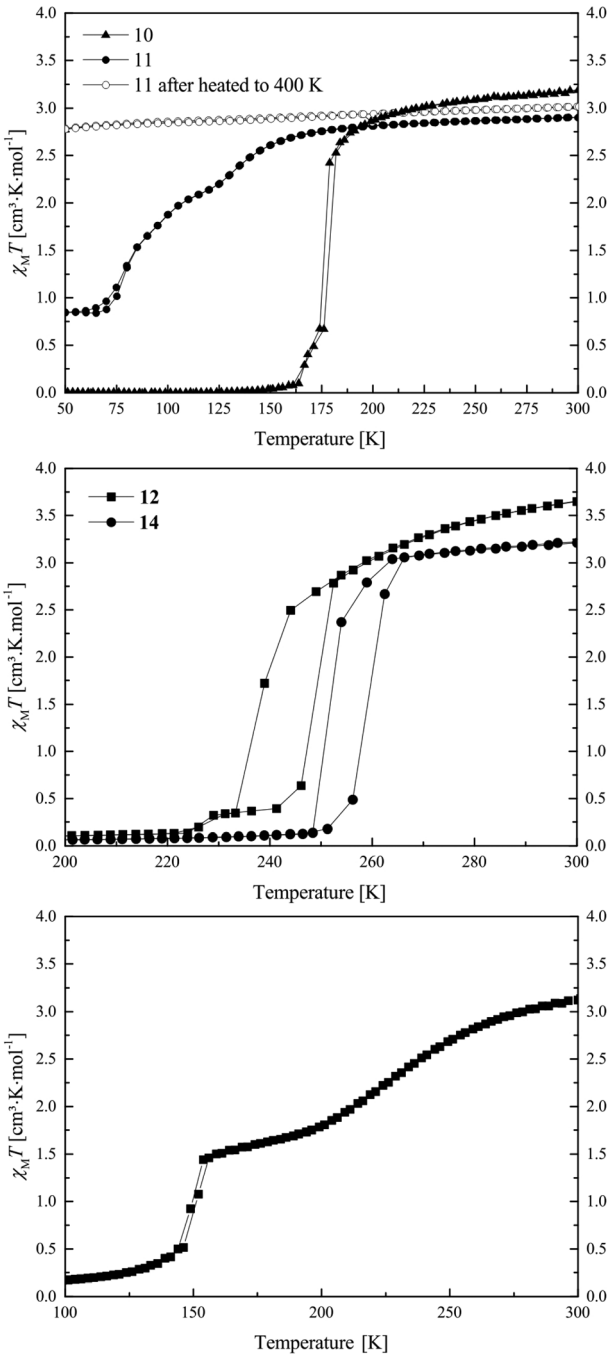

Fig. 1 Magnetic susceptibility temperature product *vs.* temperature measurement for compounds **10** and **11** (top), **12** and **14** (middle), and **15** (bottom).

Table 2 Crystallographic data of the ligand and the complexes discussed in this work

Compound	**2·0.5 H_2O·0.25 dioxane**	**6**	**10^{HS}**	**10^{LS}**	**11**	**12**	**19**	**20**
CCDC	1040379	1040378	1040374	1040375	1040380	1040376	1040375	1040377
Sum formula	$C_{46}H_{48}N_4O_{10}$	$C_{22}H_{20}FeN_2O_4$	$C_{47}H_{39}FeN_5O_4$	$C_{47}H_{39}FeN_5O_4$	$C_{37}H_{35}FeN_5O_6$	$C_{46}H_{42}FeN_4O_6$	$C_{48}H_{48}Fe_2N_4O_{13}$	$C_{44}H_{40}Fe_2N_4O_{13}$
M_r/g mol^{-1}	816.88	432.5	793.68	793.68	701.55	802.69	1000.60	944.50
Crystal system	Triclinic	Orthorhombic	Monoclinic	Monoclinic	Monoclinic	Triclinic	Triclinic	Triclinic
Space group	$P\bar{1}$	*Pbcn*	$P2_1/c$	$P2_1/c$	$P2_1/c$	$P\bar{1}$	$P\bar{1}$	$P\bar{1}$
a/Å	7.8382(10)	11.697(2)	12.179(2)	11.920(2)	28.083(5)	11.5899(7)	13.273(3)	9.027(1)
b/Å	12.3303(11)	15.864(3)	24.655(4)	24.712(4)	12.058(6)	11.9233(7)	14.292(3)	12.475(1)
c/Å	21.170(3)	10.566(2)	16.589(2)	16.280(2)	22.071(5)	14.3604(9)	14.510(3)	17.885(2)
α/°	88.110(5)	90	90	90	90	77.012(5)	63.065(15)	89.132(10)
β/°	87.730(5)	90	126.153(19)	125.183(19)	112.568(18)	88.090(5)	69.534(15)	85.598(10)
γ/°	86.920(5)	90	90	90	90	84.122(5)	78.915(16)	85.422(10)
V/Å^3	2040.4(16)	1960.6(14)	4022(2)	3919(2)	6902(3)	1923.4(2)	2297.1(9)	2001.6(4)
Z	2	4	4	4	8	2	2	2
ρ/g cm^{-3}	1.330	1.464	1.311	1.345	1.350	1.386	1.447	1.567
μ/mm^{-1}	0.094	0.801	0.426	0.437	0.490	0.449	0.702	0.801
Crystal size	0.02 × 0.09 × 0.14	0.103 × 0.114 × 0.124	0.100 × 0.163 × 0.262	0.100 × 0.163 × 0.262	0.03 × 0.100 × 0.12	0.07 × 0.100 × 0.19	0.23 × 0.24 × 0.24	0.292 × 0.309 × 0.380
T/K	100(2)	133(2)	180(2)	133(2)	175(2)	133(2)	133(2)	133(2)
λ (MoK$_\alpha$)/Å	0.71073	0.71073	0.71073	0.71073	0.71073	0.71073	0.71073	0.71073
θ-Range/°	2.6–22.0	1.28–23.74	1.65–24.59	1.60–24.60	2.252–17.31	1.455–24.584	1.6–24.6	1.638–28.064
Reflns. Collected	12 238	24 192	47 223	45 921	26 239	22 912	27 408	25 770
Indep. reflns. (R_{int})	4998 (0.074)	1858 (0.4395)	6730 (0.156)	6540 (0.165)	4159 (0.154)	6444 (0.182)	7688 (0.134)	8940 (0.104)
Parameters	541	134	514	514	403	514	604	568
R_1 (F) (all data)	0.0526 (0.1087)	0.0851 (0.1601)	0.0596 (0.1278)	0.0571 (0.1158)	0.0788 (0.1359)	0.0748 (0.1224)	0.0515 (0.1097)	0.0861 (0.1222)
wR_2	0.1299	0.1989	0.1205	0.1112	0.2073	0.1612	0.1049	0.2175
GooF	1.045	0.983	0.928	0.916	1.081	0.941	0.851	0.864

nuclear complexes of this ligand type and can be explained with the results from X-ray structure analysis.

Compound **15** exhibits at 300 K a $\chi_M T$ value of 3.12 cm^3 K mol^{-1}, corresponding to an iron(II) HS compound. Upon cooling, the sample undergoes a two-step SCO with a gradual part starting at 273 K and ending at 189 K with a T_1 of 224 K and an intermediate $\chi_M T$ value of 1.69 cm^3 K mol^{-1} (γ_{HS} = 0.54, γ_{HS} was calculated as $\gamma_{HS} = (\chi_M T(50\ K))/(\chi_M T(300\ K))$) (bottom of Fig. 1). Then the sample undergoes a second abrupt SCO step with a T_2 of 149 K. The magnetic susceptibility product remains constant with a value of 0.10 cm^3 K mol^{-1} until 10 K, which is in agreement with an iron(II) centre in the LS state. Upon several temperature cycles, the magnetic properties of **15** are stable.

X-ray structure analysis

H_2L2 (2). Suitable crystals for X-ray diffraction were obtained from a water/dioxane vapour–vapour diffusion setup.

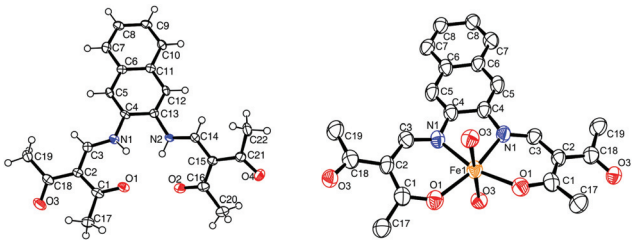

Fig. 2 ORTEP drawing of **2** (left) and **6** (right). The thermal ellipsoids are shown at the 50% level. Hydrogen atoms and solvent molecules were omitted for clarity reasons.

The structure of yellow needles of the composition **2·0.5H_2O·0.25 dioxane** was determined. Crystallographic data are summarised in Table 2. The compound crystallises in the triclinic space group $P\bar{1}$, and the asymmetric unit contains two H_2L2 molecules, a water molecule and half a dioxane solvent molecule. ORTEP drawing of a H_2L2 molecule is displayed in Fig. 2. Refinement of the ligand molecules and dioxane solvent molecule went smoothly, however the hydrogen atoms of the water molecule could not be refined. The ligand molecule can exist in two different tautomers: a keto–enamine form or an imino–enol form.

The crystal structure shows the molecule in its keto-enamine form as the C1–C2 and C15–C16 bonds can be attributed to single bonds (respectively 1.459(6) and 1.452(6)), and the C2–C3 and C14–C15 bonds can be attributed to double bonds (respectively 1.380(6) and 1.378(5)). This observation is in agreement with similar phenylene Schiff base-like ligand published in literature.[18,23] Two intramolecular hydrogen bonds are present, both between the nitrogen of the enamine and the oxygen of the ketone (Table 3). π–π interactions are present between the stacked ligand molecules, with a distance of 3.55 Å between the centroids of the first ring of the naphthalene (C4–C5–C6–C11–C12–C13). This shows that the complexes produced with this ligand have potential to also form π–π interactions.

[FeL2] (6). Suitable crystals for X-ray diffraction were obtained from the synthesis. The determination of the structure was of high interest as the elemental analysis showed that no methanol was present in the compound, and therefore a square planar coordination sphere could be assumed. The crystallographic data are summarised in Table 2. The sample crystallises in the orthorhombic space group *Pbcn*. The asym-

Table 3 Summary of the C–H···A short contacts

Compound	D	H	A	D–H	H···A	D···A	D–H···A
2·0.5 H_2O·0.25 dioxane	N1	H1	O1	0.88	1.87	2.563(5)	135
	N2	H2	O2	0.88	1.92	2.712(5)	129
	N31	H31	O31	0.88	1.93	2.566(5)	128
	N32	H32	O32	0.88	1.89	2.575(5)	133
10^{HS}	C12	H12	O3[a]	0.95	2.50	3.443(6)	169
10^{LS}	C12	H12	O3[a]	0.95	2.41	3.361(6)	174
11	C105	H105	O105[b]	0.95	2.33	3.20(2)	152
	C212	H212	O206[c]	0.95	2.36	3.22(2)	150
	C129	H129	O102[d]	0.95	2.44	3.32(2)	154
	C229	H229	O201	0.95	2.67	3.56[a]	156
	C229	H229	O202	0.95	2.67	3.27[a]	122
	C224	H224	N302[b]	0.95	2.58	3.52(2)	175
	C126	H126	N502	0.95	2.71	3.64[a]	166
	C304	H304	O203[e]	0.95	2.56	3.33(3)	139
	C501	H501	O103[f]	0.95	2.53	3.36(3)	145
12	C45	H45	O5[g]	0.95	2.70	3.24[a]	117
	C46	H46	O5[g]	0.95	2.46	3.135(7)	128
19	C20	H20A	O5[h]	0.98	2.43	3.307(7)	148
	C23	H23A	O3[i]	0.99	2.44	3.169(7)	130
20	C22	H22B	O33[j]	0.98	2.55	3.359(9)	140

a = −1 + *x*, 5/2 − *y*, −1/2 + *z*; b = *x*, 3/2 − *y*, −1/2 + *z*; c = *x*, 1/2 − *y*, −1/2 + *z*; d = 1 − *x*, 1/2 + *y*, 1/2 − *z*; e = −*x*, 1/2 + *y*, 1/2 − *z*; f = 1 − *x*, −1/2 + *y*, 1/2 − *z*; g = 1 + *x*, *y*, *z*; h = 2 − *x*, 1 − *y*, 1 − *z*; i = *x*, −1 + *y*, *z*; j = −1 + *x*, 1 + *y*, *z*. [a] Short contacts measured with mercury as the distances or angles exceed the threshold of PLATON.

Table 4 Selected bond lengths [Å] and angles [°]

	$Fe–N_{eq}$	$Fe–O_{eq}$	$Fe–L_{ax}$	$O_{eq}–Fe–O_{eq}$	$L_{ax}–Fe–L_{ax}$
6	2.095(6)	2.030(5)	2.246(5)	113.0(2)	176.06(19)
10^{HS}	2.063(4)	1.989(4)	2.138(5)	106.98(14)	174.22(17)
	2.040(4)	2.018(4)	2.226(5)		
10^{LS}	1.908(3)	1.949(3)	1.989(4)	90.49(12)	175.36(15)
	1.902(3)	1.953(3)	1.986(3)		
11	2.061(12)	2.014(10)	2.205(13)	111.5(4)	169.3(5)
	2.088(11)	2.019(10)	2.238(13)	112.6(4)	170.2(4)
	2.096(11)	2.004(10)	2.218(12)		
	2.089(11)	2.012(10)	2.276(12)		
12	1.903(4)	1.943(3)	1.996(4)	87.79(14)	173.85(16)
	1.906(4)	1.933(3)	2.004(4)		
19	2.066(4)	1.951(3)	1.771(3)	92.46(13)	148.18(19)[a]
	2.055(4)	1.965(3)	1.776(3)	92.50(13)	
	2.051(4)	1.958(3)			
	2.069(3)	1.961(3)			
20	2.037(5)	1.938(4)	1.950(4)	91.59(18)	140.9(2)[a]
	2.055(5)	1.964(4)	1.954(4)	90.18(17)	
	2.067(4)	1.954(4)			
	2.064(5)	1.950(4)			

[a] $Fe–L_{ax}–Fe$ angle.

metric unit contains half a [FeL2] complex, and the ORTEP drawing of the molecule is shown in Fig. 2. The iron centre lies in an octahedral N_2O_4 coordination sphere, the ligand serves as equatorial ligand, and as axial ligand of the neighbouring molecules through its ketone substituents, forming a 2D coordination network. Selected bonds and angles are presented in Table 4. The angle $O_{eq}–Fe–O_{eq}$ is critical in the determination of the spin state of the iron(II), as its value is about 90° in LS state and about 110° in the HS state.[24,25] The iron(II) centre is here with 113.0(2) clearly in the HS state, in agreement with its weak field coordination sphere. The 2D coordination network is located in the [101] plane, where the iron centres are connected together to form a grid.

Each 2D plane is succeeding each other along the axis [010] in a staggered fashion. Crystal packing pictures of the planes are shown in Fig. 3. Solvent accessible voids of 198.9 $Å^3$ per unit cell (10%) were found by PLATON, however no solvent was found in the structure. Voids pictures are shown in Fig. 4. Although the structure shows voids, they seem to be inaccessible to solvent molecules, as the diameter of the "channels" is only 2 Å. Perhaps small gas molecules could be inserted in the network but this study falls out of the scope of this paper. Powder diffraction proved the bulk material to be isostructural to the crystals (ESI Fig. S3†).

$[FeL3(py)_2]\cdot py$ (10), $[FeL4(py)_2]\cdot py$ (11), and $[FeL1(phpy)_2]$ (12). Suitable crystals for X-ray diffraction of compounds **10**, **11**, and **12** were obtained directly from the synthesis. The structures could be determined in the HS states for **10^{HS}** at 180 K and **11** at 175 K, and in the LS state for **10^{LS}** and **12** at 133 K. For the determination of **10^{HS}** and **10^{LS}**, the same crystal was used. In the case of **11**, although complete refinement of the crystal structure was proven difficult due to incomplete data set (θ_{max} = 17.31°) because of the low stability of the crystals, a structural motif could be obtained. The crystallographic data are summarised in Table 2. Compounds **10** and **11** crystallise in the monoclinic space group $P2_1/c$ and the compound **12** in the triclinic space group $P\bar{1}$. The asymmetric unit of **10** contains one complex molecule and one non-coordinating pyridine solvent molecule, two different iron(II) complexes and two non-coordinating solvent pyridine molecules in the case of **11**, and one complex molecule for **12**. ORTEP drawings of the asymmetric units are displayed in Fig. 5. In all structures, the iron centres lie in a N_4O_2 coordination sphere, connected to the equatorial ligand and two (phenyl)pyridine molecules. The spin state of the iron centres can be determined by the value of the $O_{eq}–Fe–O_{eq}$ angle which goes from ≈110° in the HS state to ≈90° in the LS state.[24,25] Measured $O_{eq}–Fe–O_{eq}$ angles for the HS structures (106.98(14)° for **10^{HS}**, 111.5(4)°, and 112.6(4)° for **11**) and for the LS structures (90.49(12)° for **10^{LS}** and 87.79(14)° for **12**) are in agreement with similar compounds in literature.[8,26] Selected bond lengths and angles are listed in Table 4.

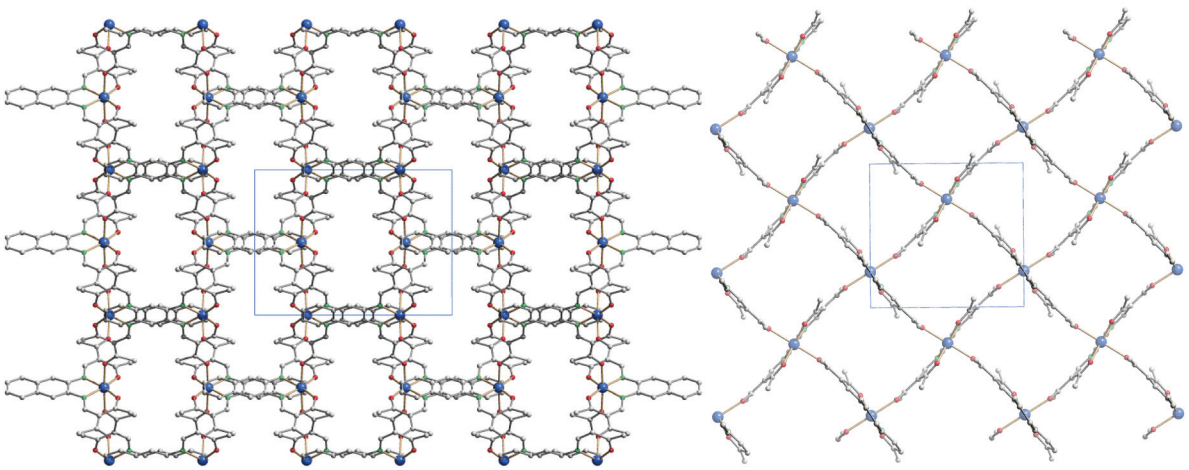

Fig. 3 Crystal packing pictures of **6** along [001] (left) and picture of a single plane along [010] (right). Hydrogen atoms were omitted for clarity.

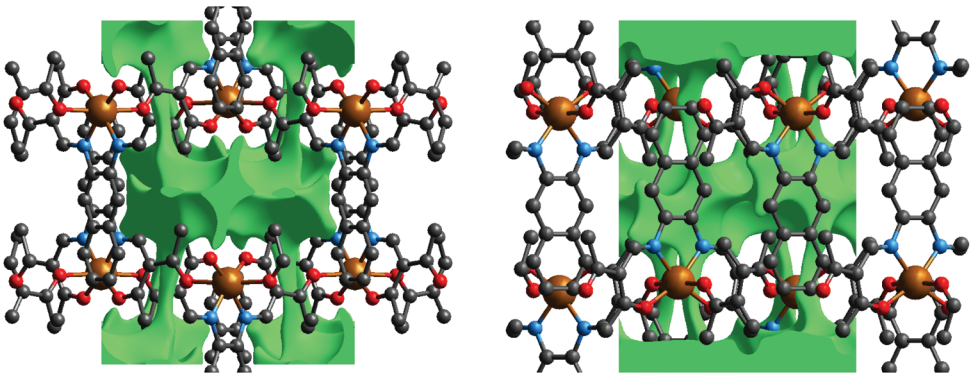

Fig. 4 Solvent accessible voids pictures of **6** along [001] (left) and [100] (right). Hydrogen atoms were omitted for clarity.

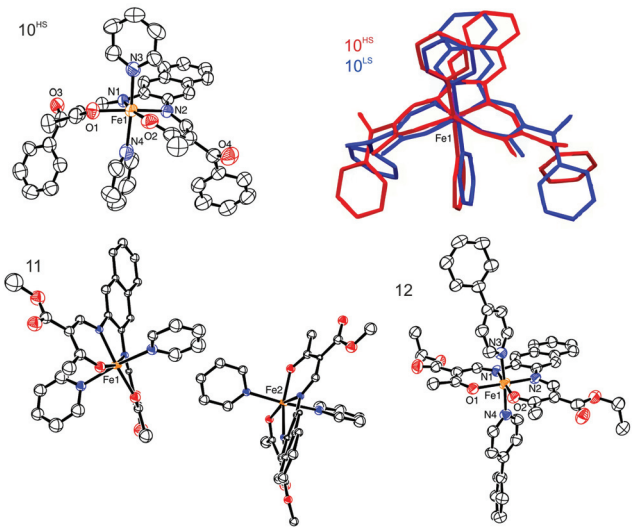

Fig. 5 ORTEP drawing **10**^{HS} (top left), **11** (bottom left), and **12** (bottom right). The thermal ellipsoids are shown at the 50% level. Hydrogen atoms and non-coordinating solvent molecules were omitted for clarity reasons. The overlay of **10**^{HS} and **10**^{LS} is represented in the top right corner.

Upon SCO, the volume of the cell of **10** is reduced by 2.5%, in agreement with the volume reduction of the coordination sphere of the iron centre as it switches from HS to LS state.[27] The complex shows a strong saddle shape with an angle of 11.54° in the HS and 10.53° in the LS state between the FeN_2O_2 plane (Fe1–N1–N2–O1–O2) and the plane containing the naphthalene cycles. The change in the saddle angle comes from changes in lengths of intermolecular contacts between the complexes. Indeed, C–H···π interactions are observed between the aromatic rings of the naphthalene and aromatic hydrogen atoms of the axial pyridine ligands, leading to the formation of 1D chains propagating along the vector [001]. Additionally, the 1D chains are linked through C–H···O bridges linking the naphthalene ring (C12–H12) to the ketone group (O3) of a neighbouring molecule, along the vector [100]. Such C–H···O bridges are known to be structure defining in many cases.[28] Contribution from both types of interactions leads to the formation of a 2D network in the *a*,*c* plane of the packing. Crystal packing and a scheme of the C–H···π interactions are shown in Fig. 6 and summarised in Tables 3 and 5. These intermolecular interactions have an influence on the slight change of the saddle angle of the molecule during SCO as the distance between the C–H and the aromatic rings partners in the interaction is increasing with the volume decrease of the coordination sphere.

The crystal packing of **11** presents a bi-layered structure: the different iron(II) complexes form planes perpendicular to vector [010], in a [Fe1Fe1–Fe2Fe2] fashion. The planes themselves are built by an intricate combination of C–H···O bridges between naphthalene and methyl ester substituents of neighbouring molecules along [001]; and, along [010], of C–H···O bridges and C–H···π interactions between axial pyridine and two neighbouring molecules. The latter C–H···O bridges connect to the oxygen atoms of the coordination sphere, which has been shown to have dramatic influence on SCO properties.[9] The two different planes (Fe1 and Fe2) actually build the same network, although similar short contacts do not have the exact same distance, especially regarding C–H···O bridges connecting to coordinating oxygen (O101, O102, O201, O202). The non-coordinating pyridine solvent molecules occupy interplanar position, binding to the planes through C–H···O and C–H···N bridges. Distances and angles of discussed short contacts are listed in Tables 3 and 5. The crystal packing of the 2D network is depicted in Fig. 7. The crystal packing of **12** is dominated by two strong interactions. Firstly, C–H···O bridges link one of the ethyl ester oxygens (O5) to a neighbouring phenylpyridine aromatic ring (C45–H45, C46–H46) and form a 1D chain of complexes along [100]. Secondly, an unusual overlap of the methyl ester group with the nearby naphthalene ring (–O6–C22═O5···π) forming pairs of complexes.[28c–f] Additional weaker stacking between adjacent phenylpyridine aromatic rings, and between naphthalene rings creates a complex network between the Fe(II) spin centres. Crystal packing pictures as well as an ORTEP representation of the –O–C═O···π

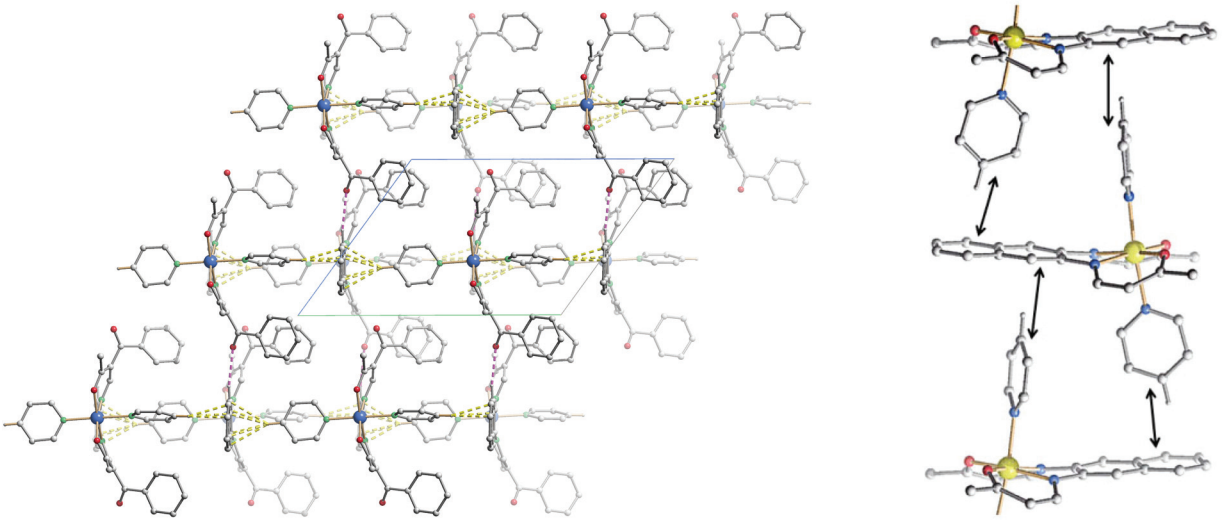

Fig. 6 Left: crystal packing of 10^{HS} along [0−10], hydrogen atoms not involved in short contacts were omitted for clarity reasons. C−H···π interactions are represented in dashed yellow lines, C−H···O in dashed pink lines. Right: excerpt of the crystal packing along [100], hydrogen atoms, non-coordinating solvent molecules, and substituents were omitted for clarity. Black double arrows indicate the C−H···π interactions positions.

Table 5 Summary of the X−Y···π interactions in crystal structures 10^{HS}, 10^{LS}, **11**, and **12**

Compound	X	Y	Cg	Y···Cg	X···Cg	X–Y···Cg
10^{HS}	C35	H35	C4–C6–C11–C13	2.41	3.358(7)	174
	C40	H40	C6–C11	2.58	3.497(8)	164
10^{LS}	C35	H35	C4–C6–C11–C13	2.42	3.364(6)	170
	C40	H40	C6–C11	2.63	3.554(5)	165
11	C131	H131	C104–C106–C111–C113	2.48	3.37(2)	156
	C231	H231	C204–C206–C211–C213	2.65	3.48(2)	147
12	C22	O5	C6–C11	3.807(4)	3.560(6)	69.1(3)

and C–H···O bridges are shown in Fig. 8, distances and angles of discussed short contacts are listed in Tables 3 and 5.

[μ-*O*-(FeL1)$_2$] (19) and [μ-*O*-(FeL4)$_2$] (20). μ-Oxido complexes are the usual oxidation product of the iron(II) complexes when in contact with oxygen. Identifying such potential side-product is critical for the good proceedings of syntheses and analyses. Crystals suitable for X-ray diffraction were obtained from slow evaporation of a methanolic solution of [FeL*x*(MeOH)$_2$] in the air. The crystallographic data are summarised in Table 2. Both compounds crystallise in the triclinic space group $P\bar{1}$, with an asymmetric unit containing one μ-oxido complex with the two iron(III) centres lying in a N_2O_3 coordination sphere. All square based pyramid iron(III) are connected through a μ-oxido bridge. The ORTEP drawing of the asymmetric units are shown in ESI, Fig. S6.† Bond lengths and angles within the coordination sphere are listed in Table 4, and are in agreement with similar published compounds.[20,24] As for the SCO complexes, C–H···O bridges between ester side substituents can be found in the crystal packings, and the complexes are stacking in column fashion. Although the conformation of the two bridged iron complexes **19** and **20** are different, the crystal packing is actually similar. Pictures of the crystal packing are shown in ESI, Fig. S7.†

Discussion

Intermolecular interactions in the crystal packing result in cooperative interactions during the spin transition. These can result in abrupt spin transitions, thermal hysteresis loops, or step-wise spin transitions. Based on the structural data a deeper understanding of the different spin crossover properties is possible.

Compound **10** shows an abrupt SCO behaviour (Fig. 1), which can be due to either to a phase transition during SCO, or due to other cooperative effects between the complexes in the solid state. The determination of the crystal structure in both spin states proved that no phase transition is involved during SCO. Cooperative interactions can arise from intermolecular contacts, and the packing of the crystal structure of **10** revealed, in both spin states, the formation of 1D chains through C–H···π interactions and C–H···O bridges between the

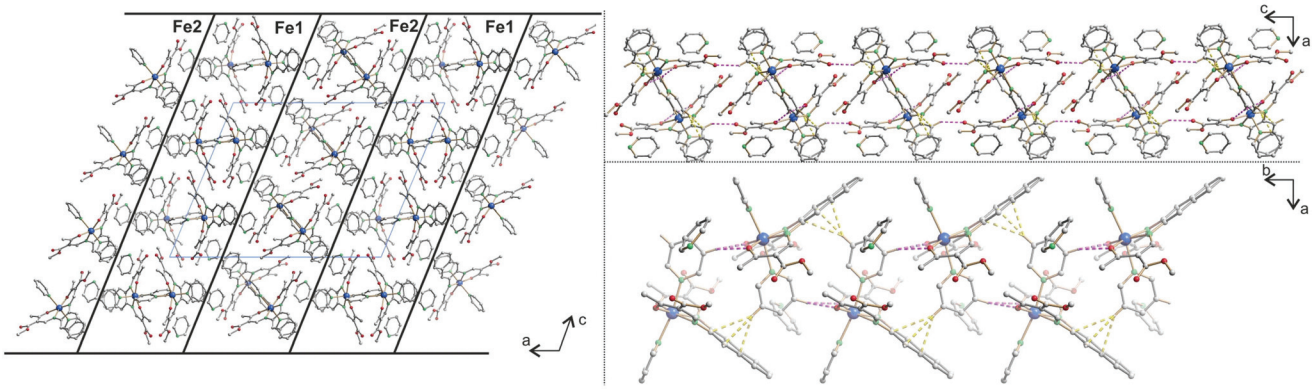

Fig. 7 Crystal packing of **11** along [010] (left), illustrating the 2D network along [010] (top right) and [001] (bottom right); hydrogen atoms not involved in short contacts were omitted for clarity reasons. C–H···π interactions are represented in dashed yellow lines, C–H···O in dashed pink lines.

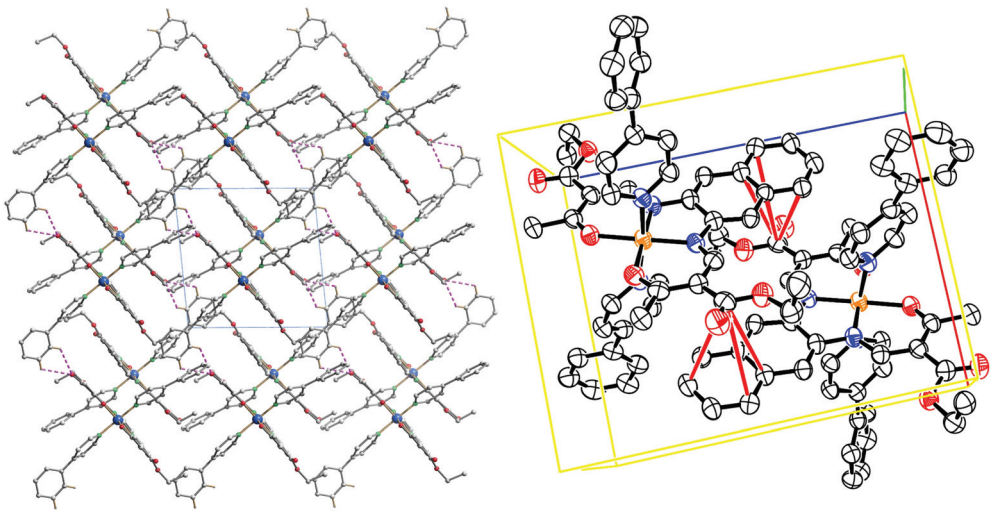

Fig. 8 Crystal packing of **12** along [001] (left); C–H···O interactions represented in dashed pink lines; ORTEP representation of the –O–C═O···π interactions, the thermal ellipsoids are shown at the 50% level. Hydrogen atoms were omitted for clarity reasons.

complexes. Thus the Schiff base-like ligand was modified successfully and π-interactions are observed and lead to cooperative interactions between the complex molecules.

Compounds **12** and **14** show both an abrupt SCO with a hysteresis of 10 K. Powder diffraction of both samples in both spin states showed that no phase transition is involved through the ST, therefore attributing the hysteresis phenomena observed to cooperative effects. The powder diffraction patterns are shown in ESI (Fig. S4–S5†). In the crystal packing of **12**, strong interactions between complexes are present, especially C–H···O bridges and –O–C═O···π interactions connect all spin centres in a 3D network. This is responsible for the high cooperativity observed for these mononuclear complexes. It would have been of course interesting to have the structure of the HS state in order to pinpoint which interaction plays a determining role in the SCO. Unfortunately the low quality and low stability of the crystal at high temperature did not allow the determination of the structure in the HS state. Powder diffractograms of **12** and **14** were compared in order to determine if the compounds are isostructural, as their SCO behaviour is very similar and just shifted in temperature. Because of the complexity of the diffractograms, arising from the low symmetry of the crystal structures, no clear conclusions can be drawn about the isostructurality of samples **12** and **14**.

Compounds **11** and **15** show both a two-step SCO. Such spin crossover are often related to different iron sites within the structure of the samples.[29] The crystal structure of **11** confirmed this hypothesis as it shows a bi-layered packing with two different iron(II) centres arranged in layers separated by layers of non-coordinating pyridine solvent molecules. As no crystals suitable for X-ray analysis could be obtained for com-

pound **15**, a room temperature Mössbauer spectrum was measured. It shows an asymmetric doublet signal with the following hyperfine parameters: δ = 0.908(6), ΔE_Q = 2.066(12) and $\Gamma/2$ = 0.174(13), which are in the region for an HS Fe(II) complex.[6,16,29] The asymmetry of the peaks is characteristic for two slightly different doublet, as the right peak is larger than the left peak. It was however not possible to correctly fit the doublet signal with two sites. The Mössbauer spectrum is presented in the ESI, Fig. S8.†

For the crystal structures of the SCO complexes discussed in this work, C–H···π interactions and C–H···O bridges strongly influence the crystal packing. For the related phenylene based complexes, only C–H···O bridges were observed.[15,16,25,29,30] The additional C–H···π interactions lead to a more frequent observation of interesting SCO properties. Out of the 10 naphthalene based complexes presented here, two showed a ST with a 10 K wide hysteresis and in two cases steps in the transition curve were observed. For comparison, for the 18 phenylene based mononuclear complexes reported so far, only one step-wise spin transition and two spin transitions with hysteresis (9 K and 70 K) were observed.[25,31,32] The 70 K hysteresis does not fit into this comparison due to the use of imidazole as axial ligand that allowed the formation of an extended N–H···O hydrogen bond network between the complexes.[31] First attempts to combine the naphthalene based Schiff base-like complexes with axial ligands suitable for the formation of hydrogen bond networks (like imidazole) are underway. The results obtained so far for the new ligands indicate that the use of an extended π-system was successful for the design of complexes with interesting SCO properties.

Experimental section

Synthesis

Methanol (MeOH) and ethanol (EtOH) were purified by distillation over magnesium under argon.[33] Toluene and pyridine were of analytical grade and degassed under argon, pyridine was kept on a 4 Å molecular sieve. Ethoxymethyleneethylacetoacetate,[34] ethoxymethyleneacetylacetone, ethoxymethylenebenzoylacetone,[34] methoxymethylenemethylacetoacetate,[18] and iron(II) acetate[35] were synthesised as described in literature. Dioxane (Sigma, 99+%), 2,3-diaminonaphthalene (Alfa Aesar, 97%), 4-(dimethylamino)pyridine (dmap; Merck, 99%) and 4-phenylpyridine (phpy; Acros, 99%) were used without further purification. All syntheses with iron(II) were carried out under argon using Schlenk tube techniques. CHN analyses were measured with a Vario El III from Elementar Analysen-Systeme. Mass spectra were recorded with a Finnigan MAT 8500 with a data system MASPEC II.

H_2L1 (1). 2,3-Diaminonaphthalene (2 g) was dissolved in 40 mL toluene. Ethoxymethyleneethylacetoacetate (5.18 g) was dissolved in 40 mL EtOH and added to the 2,3-diaminonaphthalene solution. The brown solution was stirred and refluxed for 2 hours. The mixture was then allowed to cool down to room temperature, and the solvent was removed under reduced pressure to give crude **H_2L1** as brown solid. The latter solid was dissolved in 50 mL EtOH, stirred and refluxed during 10 min, then allowed to cool down to room temperature. The beige crystals were filtered off, washed with EtOH (2 × 10 mL) and dried *in vacuo*. Yield: 3.99 g (72%). IR: $\tilde{\nu}$ = 3156(b) (NH), 1654(s) (CO), 1648(s) (CO) cm^{-1}; MS (DEI-(+), 70 eV) *m*/*z* (%): 438 (50) (H_2L1^+); elemental analysis calculated (found) for $C_{24}H_{26}N_2O_6{\cdot}C_2H_6O$ (438.47 g mol^{-1}): C 64.45 (60.41), H 5.88 (5.95), N 6.17 (5.93). ^{1}H-NMR ($CDCl_3$, 300 MHz, ppm) δ = 13.03 (d, J = 12 Hz, –NH, 2H), 8.51 (d, J = 12 Hz, =CH, 2H), 7.81 (dd, J^3 = 6 Hz, J^4 = 3 Hz, Ar–H, 2H), 7.68 (s, Ar–H, 2H), 7.50 (dd, J^3 = 6 Hz, J^4 = 3 Hz, Ar–H, 2H), 4.29 (qua, J = 7 Hz, $-CH_2-$, 4H), 2.60 (s, $-CH_3$, 6H), 1.36 (t, J = 7 Hz, $-CH_3$, 6H).

H_2L2 (2). 2,3-Diaminonaphthalene (2 g) was dissolved in 40 mL toluene. Ethoxymethyleneacetylacetone (3.96 g) was dissolved in 40 mL MeOH and added to the 2,3-diaminonaphthalene solution. The yellow solution was stirred and refluxed for 2 hours. The mixture was then allowed to cool down to room temperature, and the yellow crystals were filtered off, washed with MeOH (2 × 10 mL) and dried *in vacuo*. The crystals were recrystallized from dioxane to give pure **H_2L2**. Yield: 2 g (42%). IR: $\tilde{\nu}$ = 3223(b) (NH), 1689(s) (CO), 1675(s) (CO) cm^{-1}; MS (DEI-(+), 70 eV) *m*/*z* (%): 378 (11) (H_2L2^+); elemental analysis calculated (found) for $C_{22}H_{22}N_2O_4{\cdot}0.5C_4H_8O_2$ (422.47 g mol^{-1}): C 68.23 (67.91), H 6.20 (5.88), N 6.63 (6.89). ^{1}H-NMR ($CDCl_3$, 300 MHz, ppm) δ = 13.06 (m, –NH, 2H), 8.24 (d, J = 11 Hz, =CH, 2H), 7.83 (m, Ar–H, 2H), 7.66 (s, Ar–H, 2H), 7.53 (m, Ar–H, 2H), 2.59 (s, $-CH_3$, 6H), 2.42 (s, $-CH_3$, 6H).

H_2L3 (3). 2,3-Diaminonaphthalene (2 g) was dissolved in 40 mL toluene. Ethoxymethylenebenzoylacetone (6.51 g) was dissolved in 40 mL MeOH and added to the 2,3-diaminonaphthalene solution. The brown solution was stirred and refluxed for 2 hours. The mixture was then allowed to cool down to room temperature, and the brown crystals were filtered off, washed with MeOH (2 × 10 mL) and dried *in vacuo*. The crystals were recrystallized from MeOH to give pure **H_2L3**. Yield: 5.04 g (72%). IR: $\tilde{\nu}$ = 3204(b) (NH), 1663(s) (CO), 1598(s) (CO) cm^{-1}; MS (DEI-(+), 70 eV) *m*/*z* (%): 502 (78) (H_2L3^+); elemental analysis calculated (found) for $C_{32}H_{26}N_2O_4{\cdot}0.5CH_4O$ (518.59 g mol^{-1}): C 75.27 (74.90), H 5.442 (4.8), N 5.402 (5.377). ^{1}H-NMR ($CDCl_3$, 300 MHz, ppm) δ = 12.96 (d, J = 12 Hz, –NH, 2H), 7.92 (d, J = 12 Hz, =CH, 2H), 7.76 (m, Ar–H, 4H), 7.68 (s, Ar–H, 2H), 7.48 (m, Ar–H, 10H), 2.56 (s, $-CH_3$, 6H).

H_2L4 (4). 2,3-Diaminonaphthalene (2 g) was dissolved in 40 mL toluene. Methoxymethylenemethylacetoacetate (4.39 g) was dissolved in 40 mL MeOH and added to the 2,3-diaminonaphthalene solution. The brown solution was stirred and refluxed for 2 hours. The mixture was then allowed to cool down to room temperature, and the dark yellow crystals were filtered off, washed with MeOH (2 × 10 mL) and dried *in vacuo*. The crystals were recrystallized from MeOH to give pure **H_2L4**. Yield: 5.15 g (99%). IR: $\tilde{\nu}$ = 3265(b) (NH), 1652(s) (CO), 1622(s) (CO) cm^{-1}; MS (DEI-(+), 70 eV) *m*/*z* (%): 410 (100) (H_2L4^+); elemental analysis calculated (found) for $C_{22}H_{22}N_2O_6{\cdot}0.5CH_4O$ (426.4 g mol^{-1}): C 63.37 (62.97), H 5.672 (4.765), N 6.569

(6.592). ^{1}H-NMR ($CDCl_3$, 300 MHz, ppm) δ = 13.67 (d, J = 12 Hz, –NH, 2H), 8.57 (d, J = 12 Hz, =CH, 2H), 7.81 (dd, J^3 = 6 Hz, J^4 = 3 Hz, Ar–H, 4H), 7.68 (s, Ar–H, 2H), 7.48 (dd, J^3 = 6 Hz, J^4 = 3 Hz, Ar–H, 10H), 3.82 (s, $-CH_3$, 6H), 2.60 (s, $-CH_3$, 6H).

[FeL1(MeOH)$_2$] (5). **1** (2 g) and iron(II) acetate (0.95 g) were dissolved in 130 mL MeOH. The red suspension was stirred and refluxed for 1 hour. The mixture was then allowed to cool down to room temperature, and the brown crystals were filtered off, washed with MeOH (2 × 5 mL) and dried *in vacuo*. Yield: 1.68 g (66%). IR: $\tilde{\nu}$ = 1614(s) (CO), 1597(s) (CO) cm^{-1}; MS (DEI-(+), 70 eV) *m*/*z* (%): 492 (100) ([FeL1]$^+$); elemental analysis calculated (found) for $C_{26}H_{32}FeN_2O_8$ (556.39 g mol^{-1}): C 56.13 (55.42), H 5.80 (4.20), N 5.03 (5.20).

[FeL2] (6). **2** (2 g) and iron(II) acetate (1.1 g) were dissolved in 100 mL MeOH. The red suspension was stirred and refluxed during 1 hour. The mixture was then allowed to cool down to room temperature, and the black crystals were filtered off, washed with MeOH (2 × 5 mL) and dried *in vacuo*. Yield: 1.35 g (60%). IR: $\tilde{\nu}$ = 1685(s) (CO), 1584(s) (CO) cm^{-1}; MS (DEI-(+), 70 eV) *m*/*z* (%): 432 (100) ([FeL2]$^+$); elemental analysis calculated (found) for $C_{22}H_{20}FeN_2O_4$ (432.08 g mol^{-1}): C 61.13 (60.43), H 4.66 (4.29), N 6.48 (6.36).

[FeL3] (7). **3** (1.5 g) and iron(II) acetate (0.59 g) were dissolved in 100 mL MeOH. The red suspension was stirred and refluxed for 15 min. The mixture was then allowed to cool down to room temperature, and the black crystals were filtered off, washed with MeOH (2 × 15 mL) and dried *in vacuo*. Yield: 1.22 g (78%). IR: $\tilde{\nu}$ = 1629(s) (CO), 1575(s) (CO) cm^{-1}; MS (DEI-(+), 70 eV) *m*/*z* (%): 556 (100) ([FeL3]$^+$); elemental analysis calculated (found) for $C_{32}H_{24}FeN_2O_4$ (556.39 g mol^{-1}): C 69.08 (68.37), H 4.35 (3.44), N 5.03 (4.997). There was a miscalculation on the theoretical values.

[FeL4(MeOH)$_2$] (8). **4** (1.5 g) and iron(II) acetate (0.76 g) were dissolved in 100 mL MeOH. The red suspension was stirred and refluxed for 1 hour. The mixture was then allowed to cool down to room temperature, and the brown crystals were filtered off, washed with MeOH (2 × 5 mL) and dried *in vacuo*. Yield: 1.57 g (81%). IR: $\tilde{\nu}$ = 1620(s) (CO), 1598(s) (CO) cm^{-1}; MS (DEI-(+), 70 eV) *m*/*z* (%): 528 (100) ([FeL4]$^+$); elemental analysis calculated (found) for $C_{24}H_{28}FeN_2O_8$ (528.33 g mol^{-1}): C 54.56 (54.17), H 5.34 (5.12), N 5.30 (5.26).

[FeL2(py)$_2$]·2.5H$_2$O (9). **6** (0.2 g) were dissolved in 15 mL pyridine. The red solution was stirred and refluxed for 30 min. The mixture was then allowed to cool down and then 15 mL H_2O was added to the solution. Red crystals precipitated slowly, and the solution was left to stand at room temperature overnight. The red crystals were then filtered off, and dried *in vacuo*. Yield: 0.16 g (56%). IR: $\tilde{\nu}$ = 1612(s) (CO), 1596(s) (CO) cm^{-1}; MS (DEI-(+), 70 eV) *m*/*z* (%): 432 (100) ([FeL2]$^+$); elemental analysis calculated (found) for $C_{32}H_{35}FeN_4O_{6.5}$ (635.49 g mol^{-1}): C 60.48 (60.46), H 5.55 (3.912), N 8.82 (7.865).

[FeL3(py)$_2$]·py (10). **7** (0.2 g) were dissolved in 15 mL pyridine. The brown solution was stirred and refluxed for 30 min. The mixture was then allowed to cool down and then 15 mL H_2O was added to the solution, and the solution was left to stand at 277 K during 7 days. The black crystals were then filtered off, and dried *in vacuo*. Yield: 0.1 g (35%). IR: $\tilde{\nu}$ = 1623(s) (CO), 1584(s) (CO) cm^{-1}; MS (DEI-(+), 70 eV) *m*/*z* (%): 556 (100) ([FeL3]$^+$).

[FeL4(py)$_2$]·py (11). **8** (0.2 g) were dissolved in 15 mL pyridine. The brown solution was stirred and refluxed for 30 min. The mixture was then allowed to cool down and then 15 mL H_2O was added to the solution. Red crystals precipitated slowly, and the solution was left to stand at room temperature overnight. The red crystals were then filtered off, and dried *in vacuo*. Yield: 0.14 g (59%). IR: $\tilde{\nu}$ = 1601(s) (CO), 1582(s) (CO) cm^{-1}; MS (DEI-(+), 70 eV) *m*/*z* (%): 464 (100) ([FeL4]$^+$); elemental analysis calculated (found) for $C_{35}H_{34}FeN_5O_6$ (701.55 g mol^{-1}): C 63.34 (62.06), H 5.03 (4.59), N 9.98 (9.624).

[FeL1(phpy)$_2$] (12). **5** (0.2 g) and 4-phenylpyridine (1.67 g) were dissolved in 20 mL MeOH. The dark red suspension was stirred and refluxed for 1 hour. The mixture was then allowed to cool down and left to stand overnight at room temperature. The black crystals were then filtered off, and dried *in vacuo*. Yield: 0.06 g (21%). MS (DEI-(+), 70 eV) *m*/*z* (%): 492 (100) ([FeL1]$^+$).

[FeL2(phpy)$_2$]·2MeOH (13). **6** (0.2 g) and 4-phenylpyridine (2.16 g) were dissolved in 20 mL MeOH. The dark red solution was stirred and refluxed for 1 hour. The mixture was then allowed to cool down and left to stand overnight at room temperature. The black crystalline precipitate was then filtered off, and dried *in vacuo*. Yield: 0.22 g. IR: $\tilde{\nu}$ = 1614(s) (CO), 1587(s) (CO) cm^{-1}; MS (DEI-(+), 70 eV) *m*/*z* (%): 432 (100) ([FeL2]$^+$); elemental analysis calculated (found) for $C_{36}H_{46}FeN_4O_6$ (742.64 g mol^{-1}): C 66.97 (68.48), H 5.14 (5.74), N 7.103 (6.90).

[FeL4(phpy)$_2$] (14). **8** (0.2 g) and 4-phenylpyridine (1.76 g) were dissolved in 20 mL MeOH. The dark red solution was stirred and refluxed for 1 hour. The mixture was then allowed to cool down and left to stand overnight at room temperature. The black crystalline precipitate was then filtered off, and dried *in vacuo*. Yield: 0.18 g (61%). IR: $\tilde{\nu}$ = 1612(s) (CO), 1596(s) (CO) cm^{-1}; MS (DEI-(+), 70 eV) *m*/*z* (%): 464 (100) ([FeL4]$^+$); elemental analysis calculated (found) for $C_{44}H_{38}FeN_4O_6$ (774.64 g mol^{-1}): C 68.22 (68.68), H 4.94 (5.20), N 7.23 (7.18).

[FeL1(dmap)$_2$] (15). **5** (0.2 g) and 4-(dimethylamino)pyridine (2.44 g) were dissolved in 20 mL MeOH. The dark red solution was stirred and refluxed for 1 hour. The mixture was then allowed to cool down and left to stand overnight at room temperature. The black crystalline precipitate was then filtered off, washed with MeOH (2 × 2 mL) and dried *in vacuo*. Yield: 0.18 g (68%). IR: $\tilde{\nu}$ = 1603(s) (CO), 1574(s) (CO) cm^{-1}; MS (DEI-(+), 70 eV) *m*/*z* (%): 492 (75) ([FeL1]$^+$), 121 (100) (dmap$^+$); elemental analysis calculated (found) for $C_{38}H_{44}FeN_6O_6$ (736.64 g mol^{-1}): C 61.96 (62.35), H 6.02 (5.65), N 11.41 (11.65).

[FeL2(dmap)$_2$] (16). **6** (0.2 g) and 4-(dimethylamino)pyridine (2.44 g) were dissolved in 20 mL MeOH. The dark red solution was stirred and refluxed for 1 hour. The mixture was then allowed to cool down and left to stand overnight at room temperature. The black crystalline precipitate was then filtered off, washed with MeOH (2 × 2 mL) and dried *in vacuo*. Yield: 0.1 g

(32%). IR: $\tilde{\nu}$ = 1606(s) (CO), 1569(s) (CO) cm^{-1}; MS (DEI-(+), 70 eV) *m*/*z* (%): 431 (23) ($[FeL2]^+$), 121 (100) ($dmap^+$); elemental analysis calculated (found) for $C_{36}H_{40}FeN_6O_4$ (676.59 g mol^{-1}): C 63.91 (63.74), H 5.96 (5.69), N 12.42 (12.34).

[FeL3(dmap)$_2$] (17). **7** (0.2 g) and 4-(dimethylamino)pyridine (2.44 g) were dissolved in 20 mL MeOH. The brown solution was stirred and refluxed for 1 hour. The mixture was then allowed to cool down and left to stand overnight at room temperature. The black crystalline precipitate was then filtered off, washed with MeOH (2 × 2 mL) and dried *in vacuo*. Yield: 0.22 g (74%). IR: $\tilde{\nu}$ = 1617(s) (CO), 1583(s) (CO) cm^{-1}; MS (DEI-(+), 70 eV) *m*/*z* (%): 556 (58) ($[FeL3]^+$), 121 (100) ($dmap^+$); elemental analysis calculated (found) for $C_{46}H_{44}FeN_6O_4$ (800.72 g mol^{-1}): C 69.00 (69.73), H 5.54 (5.46), N 10.50 (10.11).

[FeL4(dmap)$_2$] (18). **8** (0.2 g) and 4-(dimethylamino)pyridine (2.44 g) were dissolved in 20 mL MeOH. The dark red solution was stirred and refluxed for 1 hour. The mixture was then allowed to cool down and left to stand overnight at room temperature. The black crystalline precipitate was then filtered off, washed with MeOH (2 × 2 mL) and dried *in vacuo*. Yield: 0.26 g (97%). IR: $\tilde{\nu}$ = 1614(s) (CO), 1596(s) (CO) cm^{-1}; MS (DEI-(+), 70 eV) *m*/*z* (%): 464 (75) ($[FeL4]^+$), 121 (100) ($dmap^+$); elemental analysis calculated (found) for $C_{36}H_{40}FeN_6O_6$ (708.58 g mol^{-1}): C 61.02 (59.20), H 5.69 (5.06), N 11.86 (11.48).

[μ-*O*-(FeL1)$_2$] (19). Suitable crystals for X-ray diffraction were obtained from slow evaporation of a solution of **5** in MeOH in the air.

[μ-*O*-(FeL4)$_2$] (20). Suitable crystals for X-ray diffraction were obtained from slow evaporation of a solution of **8** in MeOH in the air.

X-Ray structure analysis

The intensity data of **2·0.5C$_4$H$_8$O·0.5H$_2$O** were collected with a Bruker D8 Venture diffractometer, the intensity data of **5**, **10^{HS}**, **10^{LS}**, **11**, **12**, **19** and **20** were collected with a Stoe IPDS II diffractometer, both diffractometer using graphite-monochromated MoK_α radiation. The data were corrected for Lorentz and polarization effects. The structures were dissolved by direct methods (SIR-97)[36] and refined by full-matrix least-square techniques against $F_o^2 - F_c^2$ (SHELXL-97).[37] All hydrogen atoms were calculated in idealised positions with fixed displacement parameters. ORTEP-III[38] was used for the structure representation, SCHAKAL-99[39] to illustrate molecule packing and CrystalExplorer[40] for the representation of the voids. CCDC 1040373–1040380 contain the supplementary crystallographic data for this paper.

Magnetic measurements

Magnetic susceptibility data were collected using a MPMSXL-5 SQUID magnetometer under an applied field of 0.5 T over the temperature range 2 to 400 K in the settle mode. The samples were placed in gelatin capsules held within a plastic straw. The data were corrected for the diamagnetic contributions of the ligands by using tabulated Pascal's constants and of the sample holder.[41]

Conclusions

In this work we presented the synthesis of a new ligand system for iron(II) spin crossover complexes with an increased potential for the observation of π-interactions due to the extended aromatic naphthalene unit compared to the previously used benzene unit. Ten new complexes with a high potential for the observation of spin crossover were synthesised and 50% of those complexes showed the desired properties. Of those, three showed a cooperative spin transition with a maximum hysteresis width of 10 K. The X-ray structure analysis of **10** and **12** revealed C–H···π interactions, C–H···O bridges, and –O–C═O···π interactions as reason for the abrupt spin transition, with hysteresis in the case of **12**. The next step will be to extend the aromatic system further, *e.g.* by going to phenazine-derivatives[42] in order to further increase the potential for π-stacking. Another possibility is to link the naphtalene-based Schiff base-like complexes to 1D chains and by this combine rigid linkers with π-stacking. This will be part of a following paper.

Acknowledgements

Financial supports from the German Science foundation (SFB840; project A10) and the University of Bayreuth are acknowledged. We thank S. Albrecht and P. Mayer (University of Munich) for the collection of single crystal XRD date of **1a**.

Notes and references

1 (*a*) O. Kahn, *Science*, 1998, **279**, 44–48; (*b*) J.-F. Létard, P. Guionneau and L. Goux-Capes, in *Spin Crossover in Transition Metal Compounds I-III*, ed. P. Gütlich and H. Goodwin, Springer, Berlin/Heidelberg, 2004, pp. 221–249; (*c*) J. Linares, E. Codjovi and Y. Garcia, *Sensors*, 2012, **12**, 4479–4492.

2 (*a*) *Spin-Crossover Materials*, ed. M. A. Halcrow, John Wiley & Sons Ltd, Chichester, 2013; (*b*) *Spin Crossover in Transition Metal Compounds I-III*, ed. P. Gütlich and H. Goodwin, Springer, Berlin/Heidelberg, 2004, pp. 233–235.

3 (*a*) P. D. Southon, L. Liu, E. A. Fellows, D. J. Price, G. J. Halder, K. W. Chapman, B. Moubaraki, K. S. Murray, J.-F. Létard and C. J. Kepert, *J. Am. Chem. Soc.*, 2009, **131**, 10998–11009; (*b*) E. Coronado and G. Mínguez Espallargas, *Chem. Soc. Rev.*, 2013, **42**, 1525.

4 (*a*) S. Schlamp, B. Weber, A. D. Naik and Y. Garcia, *Chem. Commun.*, 2011, **47**, 7152–7154; (*b*) Y. H. Lee, A. Ohta, Y. Yamamoto, Y. Komatsu, K. Kato, T. Shimizu, H. Shinoda and S. Hayami, *Polyhedron*, 2011, **30**, 3001–3005; (*c*) J. A. Kitchen, N. G. White, C. Gandolfi, M. Albrecht, G. N. L. Jameson, J. L. Tallon and S. Brooker, *Chem. Commun.*, 2010, **46**, 6464; (*d*) K. Kuroiwa, H. Kikuchi and N. Kimizuka, *Chem. Commun.*, 2010, **46**, 1229–1231.

5 C. Gandolfi, G. G. Morgan and M. Albrecht, *Dalton Trans.*, 2012, **41**, 3726–3730.
6 B. Weber, E. S. Kaps, J. Obel, K. Achterhold and F. G. Parak, *Inorg. Chem.*, 2008, **47**, 10779–10787.
7 (*a*) W. Bauer, S. Schlamp and B. Weber, *Chem. Commun.*, 2012, **48**, 10222; (*b*) J. Linares, H. Spiering and F. Varret, *Eur. Phys. J. B*, 1999, **10**, 271–275.
8 C. Lochenie, W. Bauer, A. P. Railliet, S. Schlamp, Y. Garcia and B. Weber, *Inorg. Chem.*, 2014, **53**, 11563–11572.
9 B. Weber, W. Bauer, T. Pfaffeneder, M. M. Dîrtu, A. D. Naik, A. Rotaru and Y. Garcia, *Eur. J. Inorg. Chem.*, 2011, 3193–3206.
10 J. A. Real, A. B. Gaspar, V. Niel and M. C. Muñoz, *Coord. Chem. Rev.*, 2003, **236**, 121–141.
11 Z. J. Zhong, J.-Q. Tao, Z. Yu, C.-Y. Dun, Y.-J. Liu and X.-Z. You, *J. Chem. Soc., Dalton Trans.*, 1998, 327–328.
12 J.-F. Létard, P. Guionneau, E. Codjovi, O. Lavastre, G. Bravic, D. Chasseau and O. Kahn, *J. Am. Chem. Soc.*, 1997, **119**, 10861–10862.
13 L. Wolf and E.-G. Jäger, *Z. Anorg. Allg. Chem.*, 1966, **346**, 76–91.
14 (*a*) B. Weber, E. S. Kaps, C. Desplanches and J. Létard, *Eur. J. Inorg. Chem.*, 2008, 2963–2966; (*b*) C. Baldé, W. Bauer, E. Kaps, S. Neville, C. Desplanches, G. Chastanet, B. Weber and J. F. Létard, *Eur. J. Inorg. Chem.*, 2013, 2744–2750.
15 B. Weber, E. S. Kaps, C. Desplanches, J.-F. Létard, K. Achterhold and F. G. Parak, *Eur. J. Inorg. Chem.*, 2008, 4891–4898.
16 B. Weber, E. Kaps, J. Weigand, C. Carbonera, J.-F. Létard, K. Achterhold and F. G. Parak, *Inorg. Chem.*, 2008, **47**, 487–496.
17 (*a*) B. R. Müller, G. Leibeling and E.-G. Jäger, *Mol. Cryst. Liq. Cryst. Sci. Technol., Sect. A*, 1999, **334**, 389–394; (*b*) B. Weber and E.-G. Jäger, *Z. Anorg. Allg. Chem.*, 2009, **635**, 130–133; (*c*) S. Thallmair, W. Bauer and B. Weber, *Polyhedron*, 2009, **28**, 1796–1801.
18 W. Bauer, T. Ossiander and B. Weber, *Z. Naturforsch., B: Chem. Sci.*, 2010, 323–328.
19 S. Schlamp, P. Thoma and B. Weber, *Eur. J. Inorg. Chem.*, 2012, 2759–2768.
20 S. Schlamp, P. Thoma and B. Weber, *Chem. – Eur. J.*, 2014, **20**, 6462–6473.
21 (*a*) W. Bauer, C. Lochenie and B. Weber, *Dalton Trans.*, 2014, **43**, 1990–1999; (*b*) B. Weber and J. Obel, *Z. Anorg. Allg. Chem.*, 2009, **635**, 2474–2479.
22 B. Weber, J. Obel, D. Henner-Vasquez and W. Bauer, *Eur. J. Inorg. Chem.*, 2009, 5527–5534.
23 C. Lochenie, S. Schlamp, A. P. Railliet, K. Robeyns, B. Weber and Y. Garcia, *CrystEngComm*, 2014, **16**, 6213.
24 B. Weber and E.-G. Jäger, *Eur. J. Inorg. Chem.*, 2009, 465–477.
25 B. Weber, *Coord. Chem. Rev.*, 2009, **253**, 2432–2449.
26 S. Schlamp, K. Dankhoff and B. Weber, *New J. Chem.*, 2014, **38**, 1965–1972.
27 P. Guionneau, M. Marchivie, G. Bravic, J.-F. Létard and D. Chasseau, in *Spin Crossover in Transition Metal Compounds I–III*, ed. P. Gütlich and H. Goodwin, Springer, Berlin/Heidelberg, 2004, vol. II, p. 785.
28 (*a*) T. Steiner and G. R. Desiraju, *Chem. Commun.*, 1998, 891–892; (*b*) G. R. Desiraju, *Acc. Chem. Res.*, 2002, **35**, 565–573; (*c*) J. E. Gautrot, P. Hodge, D. Cupertino and M. Helliwell, *New J. Chem.*, 2006, **30**, 1801–1807; (*d*) R. J. Santos-Contreras, F. J. Martínez-Martínez, E. V. García-Báez, I. I. Padilla-Martínez, A. L. Peraza and H. Höpfl, *Acta Crystallogr., Sect. C: Cryst. Struct. Commun.*, 2007, **63**, o239–o242; (*e*) F. H. Allen, C. A. Baalham, J. P. M. Lommerse and P. R. Raithby, *Acta Crystallogr., Sect. B: Struct. Sci.*, 1998, **54**, 320–329; (*f*) T. J. Mooibroek, P. Gamez and J. Reedijk, *CrystEngComm*, 2008, **10**, 1501–1515.
29 B. Weber, C. Carbonera, C. Desplances and J.-F. Létard, *Eur. J. Inorg. Chem.*, 2008, 1589–1598.
30 B. Weber, E. Kaps, J. Obel and W. Bauer, *Z. Anorg. Allg. Chem.*, 2008, **634**, 1421–1426.
31 B. Weber, W. Bauer and J. Obel, *Angew. Chem., Int. Ed.*, 2008, **47**, 10098–10101.
32 C. Lochenie, W. Bauer, S. Schlamp, P. Thoma and B. Weber, *Z. Anorg. Allg. Chem.*, 2012, **638**, 98–102.
33 H. G. O. Becker, Organikum, *Organisch-chemisches Grundpraktikum*, Johann Ambrosius Barth, Berlin, 19th edn, 1993.
34 L. Claisen, *Justus Liebigs Ann. Chem.*, 1897, **297**, 1–98.
35 B. Weber, R. Betz, W. Bauer and S. Schlamp, *Z. Anorg. Allg. Chem.*, 2011, **637**, 102–107.
36 A. Altomare, M. C. Burla, M. Camalli, G. L. Cascarano, C. Giacovazzo, A. Guagliardi, A. G. G. Moliterni, G. Polidori and R. Spagna, *J. Appl. Crystallogr.*, 1999, **32**, 115–119.
37 G. Sheldrick, *Acta Crystallogr., Sect. A: Fundam. Crystallogr.*, 2008, **64**, 112–122.
38 (*a*) C. K. Johnson and M. N. Burnett, *ORTEP-III*, Oak-Ridge National Laboratory, Oak-Ridge, TN, 1996; (*b*) L. Farrugia, *J. Appl. Crystallogr.*, 1997, **30**, 565.
39 E. Keller, *Schakal-99*, University of Freiburg, Freiburg, Germany, 1999.
40 (*a*) S. K. Wolff, D. J. Grimwood, J. J. McKinnon, M. J. Turner, D. Jayatilaka and M. A. Spackmann, *Crystal-Explorer*, University of Wesertn Australia, 2012; (*b*) M. J. Turner, J. J. McKinnon, D. Jayatilaka and M. A. Spackman, *CrystEngComm*, 2011, **13**, 1804.
41 O. Kahn, *Molecular Magnetism*, VCH, New York, N.Y, 1993.
42 C. Lochenie, K. G. Wagner, M. Karg and B. Weber, *J. Mater. Chem. C*, 2015, **3**, 7925–7935.